# LETTER TO THE EDITOR

# Determination of Oxygen Atomic Positions in a Ga–In–Sn–O Ceramic Using Direct Methods and Electron Diffraction

W. Sinkler,[*,1] L. D. Marks,[*] D. D. Edwards,[*] T. O. Mason,[*] K. R. Poeppelmeier,[†]
Z. Hu,[‡] and J. D. Jorgensen[‡]

[*]Department of Materials Science and Engineering, Northwestern University, 2225 Sheridan Rd., Evanston, Illinois 60208-3108;
[†]Department of Chemistry, Northwestern University, 2145 Sheridan Rd., Evanston, Illinois 60208-3113; [‡]Argonne National Laboratory, Argonne, Illinois 60439

**Direct methods using dynamical transmission electron diffraction (TED) intensities is applied to the solution of $(Ga,In)_2SnO_5$. Dynamical diffraction effects in the TED data lead to an emphasis of oxygen positions in the structure. Application of direct methods to dynamical diffraction intensities represents a valuable new technique for obtaining approximate atom positions of light elements in ceramics using an experiment which is simple to perform and does not require a single crystal.** © 1998 Academic Press

At present, the most common methods for solving inorganic crystal structures rely on diffraction data combined with numerical refinement of atomic positions. However, refinement procedures such as Rietveld are model-dependent, and can only succeed given an initial set of atomic positions which is reasonably close to the actual structure. One of the few techniques which can directly provide real-space information on atomic positions is high resolution transmission electron microscopy (HRTEM). Under optimal imaging conditions with a thin specimen, it is now routine to obtain structure images to a resolution of about 1.8 Å. While this is small enough to image the heavier cations in ceramic materials, HRTEM images generally do not contain directly interpretable information concerning light atom positions. An additional means of obtaining direct, real space information concerning atom positions are so-called direct methods (1). Direct methods rely on diffraction information alone, and extract the missing phase information using statistical relationships among the structure factors. While the requirement of complete kinematical data sets has largely limited previous application of

direct methods to cases in which single crystal X-ray data could be obtained, recent work combining TED with direct methods has indicated that significant dynamical distortion of intensities, as well as incompleteness of data, may be tolerated. Nevertheless, all previous combinations of TED and direct methods have attempted to avoid dynamical effects in the data, and the direct methods results have been interpreted within a kinematical approximation (2–8). In the present work, direct methods are applied to TED data from a compound containing strongly scattering elements, in which dynamical effects are unavoidably dominant. The dynamical effects, far from being detrimental to obtaining structural information, led to a useful emphasis of oxygen atom positions in the compound.

The Ga–In–Sn–O ternary oxide system is currently under investigation for potential transparent conducting oxide materials which are used in flat panel displays. In the course of the investigation, several previously unreported phases have been found (9, 10). The $(Ga,In)_2SnO_5$ sample herein was initially identified using powder X-ray diffraction, which indicated a monoclinic unit cell with $a = 11.69$, $b = 3.17$, $c = 10.73$ Å, and $\beta = 99.00°$. The short $b$-axis and monoclinic symmetry suggest that $(Ga,In)_2SnO_5$ is structurally related to a series of intergrowth compounds expressed as $Ga_4M_{m-4}O_{2m-2}$, ($M$ = Ti, Sn, or Ge and $m$ an odd integer) (11). However, unlike the previously reported $\beta$-gallia/rutile intergrowth structures, $(Ga,In)_2SnO_5$ corresponds to an even member ($m = 6$) of the series.

Figure 1 is an HRTEM image of the $(Ga,In)_2SnO_5$ crystal taken along the $b$-axis. The defocus of the image was estimated at $-500$ Å, which is slightly below Scherzer defocus for the instrument used (a Hitachi H9000), but still within the extended Scherzer interval in which no sign reversal of the contrast transfer function occurs to beyond $0.45$ Å$^{-1}$. Within the weak phase object approximation, areas of large

[1] To whom correspondence should be addressed. E-mail: w-sinkler@nwu.edu.
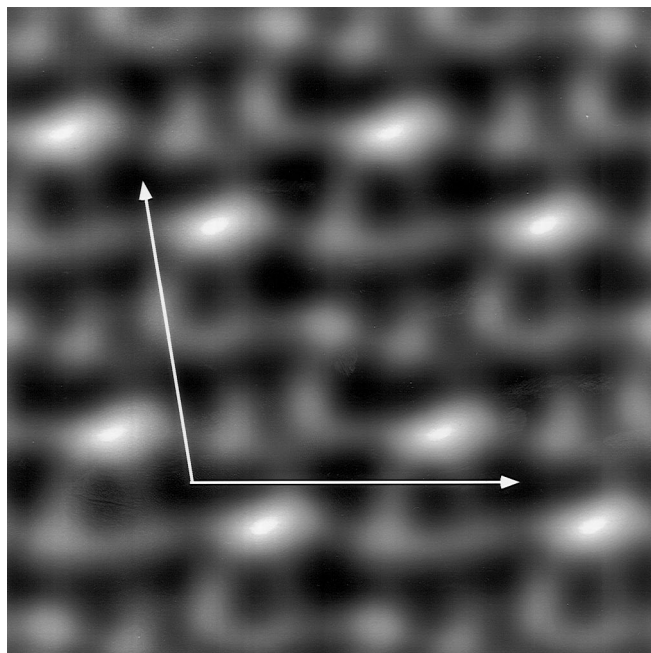
**FIG. 1.** HRTEM image of $(Ga,In)_2SnO_5$ at $-500$ Å defocus showing projected unit cell. The image has been processed by averaging several unit cells.



○ oxygen    ● tin

○ gallium    ◐ indium/gallium

**FIG. 2.** Structure of $(Ga,In)_2SnO_5$ viewed along [010].

negative potential appear dark at this defocus, and one may thus use the image to obtain approximate positions of the heavier cations of the structure. This is shown in Table 1, in which cation positions estimated from Fig. 1 are compared with those from refinement of neutron powder diffraction data which was used to confirm the structure (see Fig. 2).
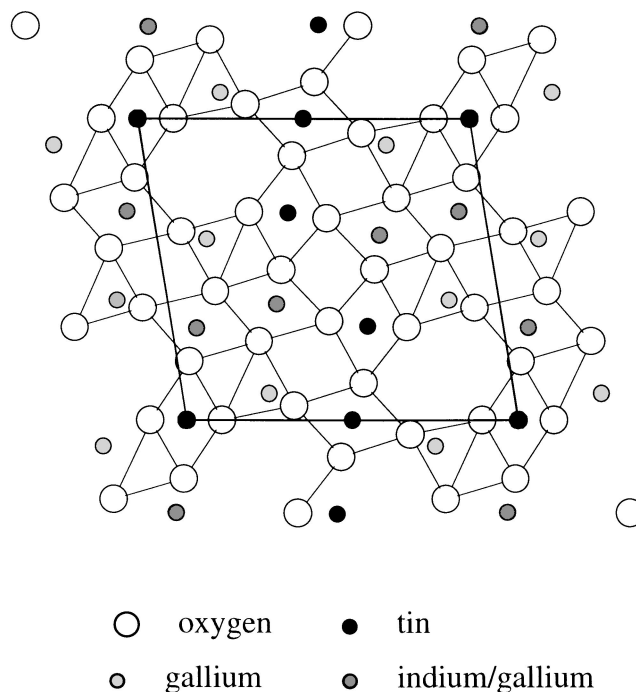
Although the HRTEM image is limited in the accuracy of the cation positions, and does not allow oxygen atom positions to be determined, it does provide information at low resolution ($\leq 0.45$ Å$^{-1}$) concerning the phases of

**TABLE 1**
**Cation Positions from HRTEM and Neutron Diffraction**

| Atom | $r_{HREM}$ | | $r_{neutron}$ | | | $\Delta r$ [Å] |
| | $x$ | $z$ | $x$ | $y$ | $z$ | |
|---|---|---|---|---|---|---|
| Sn1 | 0.0 | 0.0 | 0.0 | 0.0 | 0.0 | — |
| Sn2 | 0.515 | 0.062 | 0.5 | 0.0 | 0.0 | 0.66 |
| Sn3 | 0.594 | 0.320 | 0.5918(6) | 0.5 | 0.3112(7) | 0.10 |
| In/Ga1[a] | 0.305 | 0.360 | 0.3281(6) | 0.0 | 0.3859(7) | 0.35 |
| In/Ga2[b] | 0.078 | 0.328 | 0.0756(8) | 0.5 | 0.3053(9) | 0.24 |
| Ga1 | 0.172 | 0.672 | 0.1500(5) | 0.0 | 0.6022(6) | 0.75 |
| Ga2 | 0.234 | 0.031 | 0.2624(5) | 0.5 | 0.0869(5) | 0.64 |

[a] Indium occupancy 0.48.

[b] Indium occupancy 0.72.

crystallographic structure factors. This information can be of significatnt advantage to direct methods calculations. An accurate estimate of the oxygen atom positions was obtained by combining low resolution phase information from the HRTEM image with direct methods using strongly dynamical TED intensities. For direct phasing, TED intensities were collected using a Hitachi HF2000 field-emission TEM. A small spot size was used in order to gather data representing a single specimen thickness. Data were collected on photographic film, and quantification and scaling was performed as presented previously (12). The diffraction data set consisted of 81 nonequivalent beams, to a resolution of 0.9 Å$^{-1}$. Phases were determined from the Fourier transform of the HRTEM image in Fig. 1, using the following guidelines:

1. phase deviating less than 25° from 0° or 180° (expected from centrosymmetry);

2. spatial frequency less than 0.45 Å$^{-1}$;

3. amplitude greater than 5% that of strongest beam in the HRTEM power spectrum.

This allowed fixing of phases for 17 of the strongest beams in the diffraction data set, and one additional strong beam was fixed based on a strong $\Sigma_1$ phase indication.

The direct methods calculation used a genetic algorithm to fix eight additional phases (13), and phase extension based on a minimum entropy approach (14). The top 20 solutions, ranked using a figure of merit, fell into three categories. Figure 3 shows an example of the first category
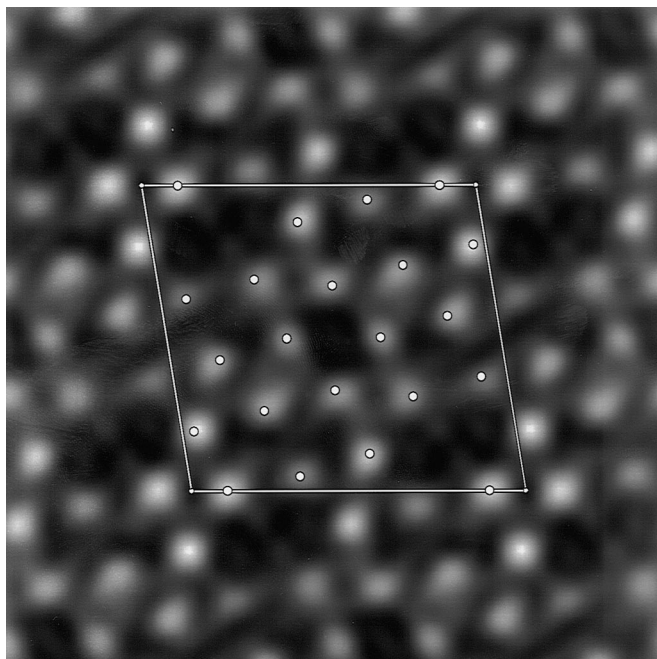
**FIG. 3.** Direct methods solution using electron diffraction intensities to a resolution of 0.9 Å$^{-1}$. The solution uniquely shows peaks at all oxygen atom positions (dots).

**TABLE 2**
**Oxygen Positions from Direct Methods and Neutron Diffraction Atom**

| Atom | $r_{\text{direct methods}}$ | | $r_{\text{neutron}}$ | | | $\Delta r$ [Å] |
|------|------|------|------|------|------|------|
|      | $x$ | $z$ | $x$ | $y$ | $z$ |  |
| O1 | 0.329 | 0.048 | 0.3320(7) | 0.0 | 0.0472(8) | 0.04 |
| O2 | 0.046 | 0.203 | 0.0365(6) | 0.0 | 0.1941(8) | 0.13 |
| O3 | 0.485 | 0.313 | 0.4789(7) | 0.0 | 0.3245(8) | 0.13 |
| O4 | 0.688 | 0.312 | 0.7096(6) | 0.0 | 0.3076(6) | 0.25 |
| O5 | 0.126 | 0.421 | 0.1490(7) | 0.0 | 0.4287(9) | 0.27 |
| O6 | 0.108 | 0.00 | 0.1081(7) | 0.5 | 0.0003(7) | 0.01 |
| O7 | 0.545 | 0.110 | 0.5515(7) | 0.5 | 0.1209(8) | 0.13 |
| O8 | 0.266 | 0.281 | 0.2570(6) | 0.5 | 0.2617(8) | 0.22 |
| O9 | 0.359 | 0.499 | 0.3586(6) | 0.5 | 0.4987(7) | 0.00 |
| O10 | 0.063 | 0.640 | 0.0768(7) | 0.5 | 0.6272(8) | 0.19 |

(9 of the top 20 solutions). The image has 20 sharp maxima in the unit cell, in agreement with the number of oxygen atoms. In addition, the peaks show groups which are identifiable as projected octahedra and tetrahedra, and are thus reasonable based on expected octahedral coordination for the tins and gallium/indium atoms, and tetrahedral coordination for gallium. By assuming that the peaks in Fig. 3 are oxygen positions, and combining these with the HRTEM image for the cation positions, the basic features of a plausible structure may be determined (the oxygen positions indicating in addition the cation ordering). In order to confirm the structure, NPD data were collected at Argonne National Laboratory's Intense Pulsed Neutron Source, and refined using GSAS code (15). Peak positions from Fig. 3 were used as initial oxygen positions in refinement of the NPD data ($R_p = 0.0495$). The initial and final oxygen positions are compared in Table 2, and show agreement to within 0.27 Å.

The other two sets of phasing solutions also showed a relationship to the structure. The second set (seven solutions), while streaked in appearance compared to Fig 3, had maxima at all cation positions, while the third set had a more inhomogeneous intensity distribution, with sharp peaks at a subset of five cation positions, and two additional peaks without a clear relationship to the structure. The tendency for solutions to show either oxygen or cation positions is explainable by separating the diffraction data

set into low- and high-order reflections, as shown schematically in Fig. 4a. By performing direct phasing on data truncated to 0.4 Å$^{-1}$, corresponding to region A of Fig. 4a, the top-ranked solutions are all similar to that shown in Fig. 4b, and uniquely show peaks at the cation positions. This suggests that the beams from region A, when considered alone, are consistent with a real space distribution $M$ which is peaked at the cations, and is thus pseudo-kinematical. The appearance of oxygen positions in Fig. 3 thus indicates that the more dynamical high-order beams of region B contain a negative or canceling component $-M$ at the metal ions and a positive component O at the oxygen positions, so that A+B has peaks at oxygen positions. However, an additional solution found by the phasing algorithm is a subtraction of B, which instead of canceling further amplifies the cation peaks inherent in region A. This explains why the direct methods solutions using the full data set may reflect either the oxygen or the cation structure, corresponding to in-phase and out-of-phase combinations of regions A and B.

The TED data represent the modulus squared of the complex specimen exit wave's ($\psi(\mathbf{r})$) Fourier transform. As is explained in detail elsewhere (16), in applying direct methods to obtain a real solution the function being restored is, to a good approximation, the modulus of the Babinet, or $|1 - \psi(\mathbf{r})|$. Figure 5 shows $|1 - \psi(\mathbf{r})|$ calculated using multislice for a thickness of 113 Å and resolution to 1.0 Å$^{-1}$. As can be seen, Fig. 5 has peaks at all oxygen positions and cancellation at cation positions, and thus resembles the phasing solution in Fig 3. Atom-like peaks at oxygen positions are found in $|1 - \psi(\mathbf{r})|$ over a broad range of thickness from 50 to 300 Å (16). This feature of the dynamical exit wave accounts for the sensitivity of direct methods for light atoms when combined with strongly dynamical TED data. The occurrence of peaks in $|1 - \psi(\mathbf{r})|$ at atom positions, as well as the particular prominence of light
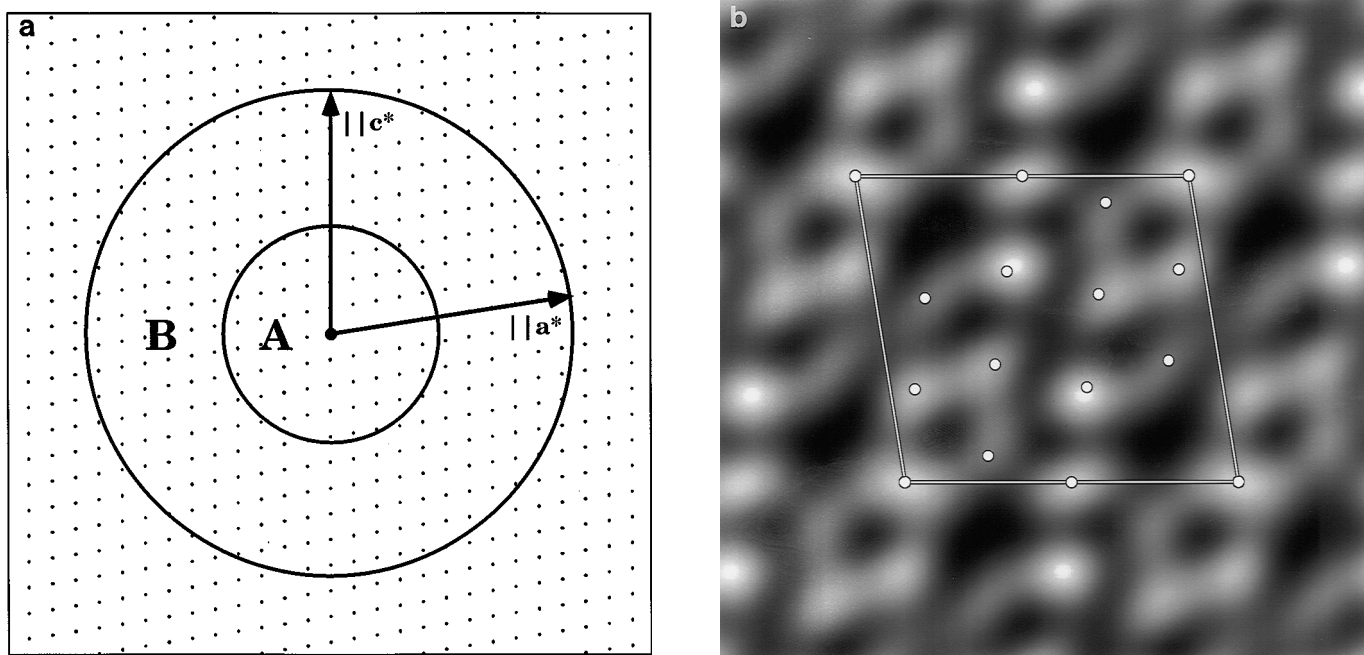
**FIG. 4.** (a) Schematic representation of the reciprocal lattice plane for $(Ga,In)_2SnO_5$ in a [010] projection. Circles are at 0.4 and 0.9 $\text{Å}^{-1}$. (b) Direct methods solution to a resolution of 0.4 $\text{Å}^{-1}$. Dots in (b) indicate neutron-refined cation positions. Strong peaks are observed at the sites of the heavier Sn and In/Ga cation sites, while weaker peaks are present at the Ga sites.

atoms, follows from electron channeling theory (17, 18), and is a general feature in structures such as the present one which consist of well-resolved atomic columns (16).
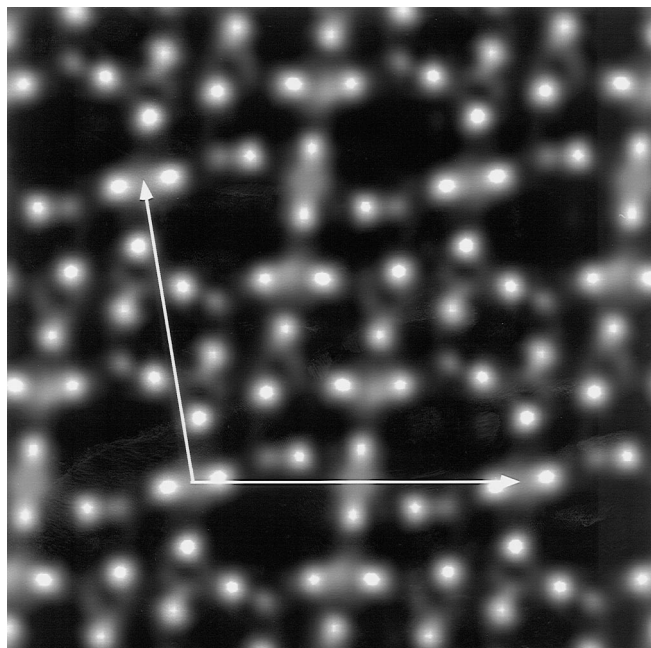


**FIG. 5.** Scattered dynamical exit wave modulus $|\psi(\mathbf{r}) - 1|$ calculated using multislice for 113 Å thickness and 1 $\text{Å}^{-1}$ resolution. Predominant peaks occur at the oxygen atomic positions.

The present work indicates that direct methods may be used with TED data, combined with phase information from HRTEM, to obtain accurate estimates of light atom positions. The approach is expected to work as long as the light atoms are well resolved in projection. Because the technique is easy to apply and uses widely available equipment, it may be of significant value to solid state chemists in determining starting positions for structure refinement of newly synthesized compounds. In addition to the structure presented here, an additional Ga–In–Sn–O structure, $(Ga,In)_4Sn_3O_{12}$, was recently solved. The sensitivity for light atoms derives from the dynamical cancellation at heavier cation positions in foils of intermediate thickness. Because it uses electron radiation, an additional strength of the technique is its applicability to problems in which a single-phase sample cannot be obtained. In such cases the present technique can provide initial atomic positions for subsequent refinement by quantitative HRTEM (19) or refinement of electron diffraction intensities (20).

### ACKNOWLEDGMENTS

## REFERENCES

1. M. Woolfson and H.-F. Fan, "Physical and Non-Physical Methods of Solving Crystal Structures." Cambridge Univ. Press, Cambridge, UK, 1995.
2. H.-F. Fan, S. B. Xiang, F. H. Li, Q. Pan, N. Uyeda, and Y. Fujiyoshi, *Ultramicroscopy* **36,** 361 (1991).
3. J. J. Hu, F. H. Li, and H. F. Fan, *Ultramicroscopy* **41,** 387 (1992).
4. W. Dong, T. Baird, J. R. Fryer, C. J. Gilmore, D. D. MacNicol, G. Bricogne, D. J. Smith, M. A. O'Keefe, and S. Hovmöller, *Nature* **355,** 605 (1992).
5. C. J. Gilmore, K. Shankland, and G. Bricogne, *Proc. R. Soc. London Sect. A* **442,** 97 (1993).
6. D. L. Dorset, *Acta Crystallogr. Sect. A* **52,** 753 (1996).
7. L. D. Marks, R. Plass, and D. L. Dorset, *Surf. Rev. Lett.* **4,** 1 (1997).
8. C. Collazo-Davila, L. D. Marks, K. Nishii, and Y. Tanishiro, *Surf. Rev. Lett.* **4,** 65 (1997).
9. D. D. Edwards and T. O. Mason, submitted for publication.
10. D. D. Edwards, T. O. Mason, W. Sinkler, L. D. Marks, F. Goutenoire, and K. R. Poeppelmeier, submitted for publication.
11. L. A. Bursill and G. G. Stone, *J. Solid State Chem.* **38,** 149 (1981).
12. P. Xu, G. Jayaram, and L. D. Marks, *Ultramicroscopy* **53,** 15 (1994).
13. E. Landree, C. Collazo-Davila, and L. D. Marks, *Acta Crystallogr. Sect. B*, in press.
14. L. D. Marks and E. Landree, *Acta Crystallogr. Sect. A*, in press.
15. A. L. Larsen and R. B. von Dreele, General Structure Analysis System, LAUR 86-748, Los Alamos National Laboratory, 1985–1990.
16. W. Sinkler, E. Bengu, and L. D. Marks, submitted for publication.
17. F. Fujimoto, *Phys. Stat. Sol.* **45,** 99 (1978).
18. D. Van Dyck and M. Op de Beeck, *Ultramicroscopy* **64,** 99 (1996).
19. H. Zhang, L. D. Marks, Y. Y. Wang, H. Zhang, V. P. Dravid, P. Han, and D. A. Payne, *Ultramicroscopy* **57,** 103 (1995).
20. H. W. Zandbergen, J. Jansen, R. J. Cava, J. J. Krajewski, and W. F. Peck, *Nature* **372,** 759 (1994).